



Universidad Pontificia Comillas (ICAI)
Master in Safety and Mobility Engineering

MASTER'S THESIS

**Long Bone Properties Variation as a function of age:
mechanical and compositional characterization**

Author: Claudia Vázquez Sanz
Principal Instructor: Francisco J. López Valdés
Secondary Instructor: Elena María Tejado Garrido

2022

Madrid

AUTHORIZATION FOR DIGITALIZATION, STORAGE AND DISSEMINATION IN THE NETWORK OF END-OF-DEGREE PROJECTS, MASTER PROJECTS, DISSERTATIONS OR BACHILLERATO REPORTS

I. Declaration of authorship and accreditation thereof.

The author Mr. JMS. Claudia Vázquez Sanz

HEREBY DECLARES that he/she owns the intellectual property rights regarding the piece of work:

“Long Bone Properties Variation as a function of age: mechanical and compositional characterization” that this is an original piece of work, and that he/she holds the status of author, in the sense granted by the Intellectual Property Law.

2. Subject matter and purpose of this assignment.

With the aim of disseminating the aforementioned piece of work as widely as possible using the University's Institutional Repository the author hereby GRANTS Comillas Pontifical University, on a royalty-free and non-exclusive basis, for the maximum legal term and with universal scope, the digitization, archiving, reproduction, distribution and public communication rights, including the right to make it electronically available, as described in the Intellectual Property Law. Transformation rights are assigned solely for the purposes described in a) of the following section.

3. Transfer and access terms

Without prejudice to the ownership of the work, which remains with its author, the transfer of rights covered by this license enables:

- a) Transform it in order to adapt it to any technology suitable for sharing it online, as well as including metadata to register the piece of work and include "watermarks" or any other security or protection system.
- b) Reproduce it in any digital medium in order to be included on an electronic database, including the right to reproduce and store the work on servers for the purposes of guaranteeing its security, maintaining it and preserving its format.
- c) Communicate it, by default, by means of an institutional open archive, which has open and costfree online access.
- d) Any other way of access (restricted, embargoed, closed) shall be explicitly requested and requires that good cause be demonstrated.
- e) Assign these pieces of work a Creative Commons license by default.
- f) Assign these pieces of work a HANDLE (persisteni URL). by default

4. Copyright.

The author, as the owner of a piece of work, has the right to:

- a) Have his/her name clearly identified by the University as the author
- b) Communicate and publish the work in the version assigned and in other subsequent versions using any medium.
- c) Request that the work be withdrawn from the repository for just cause. d) Receive reliable communication of any claims third parties may make in relation to the work and, in particular, any claims relating to its intellectual property rights.

5. Duties of the author.

The author agrees to:

- a) Guarantee that the commitment undertaken by means of this official document does not infringe any third party rights, regardless of whether they relate to industrial or intellectual property or any other type.
- b) Guarantee that the content of the work does not infringe any third party honor, privacy or image rights.
- c) Take responsibility for all claims and liability, including compensation for any damages, which may be brought against the University by third parties who believe that their rights and interests have been infringed by the assignment.
- d) Take responsibility in the event that the institutions are found guilty of a rights infringement regarding the work subject to assignment

6. Institutional Repository purposes and functioning.

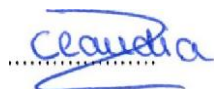
The work shall be made available to the users so that they may use it in a fair and respectful way with regards to the copyright, according to the allowances given in the relevant legislation, and for study or research purposes, or any other legal use. With this aim in mind, the University undertakes the following duties and reserves the following powers:

- a) The University shall inform the archive users of the permitted uses; however, it shall not guarantee or take any responsibility for any other subsequent ways the work may be used by users, which are non-compliant with the legislation in force. Any subsequent use, beyond private copying, shall require the source to be cited and authorship to be recognized, as well as the guarantee not to use it to gain commercial profit or carry out any derivative works.
- b) The University shall not review the content of the works, which shall at all times fall under the exclusive responsibility of the author and it shall not be obligated to take part in lawsuits on behalf of the author in the event of any infringement of intellectual property rights deriving from storing and archiving the works. The author hereby waives any claim against the University due to any way the users may use the works that is not in keeping with the legislation in force,

- c) The University shall adopt the necessary measures to safeguard the work in the future.
- d) The University reserves the right to withdraw the work, after notifying the author, in sufficiently justified cases, or in the event of third party claims.

Madrid, on 14.... of..... July 2022.....,

HEREBY ACCEPTS Claudia Vázquez Sanz

A handwritten signature in blue ink that reads "claudia". The signature is written in a cursive style and is positioned above a horizontal dotted line.

Reasons for requesting the restricted, closed or embargoed access to the work in the Institution's

Repository

Declaro, bajo mi responsabilidad, que el Proyecto presentado con el título

"Long Bone Properties Variation as a function of age: mechanical and compositional characterization" en la ETS de Ingeniería - ICAI de la Universidad Pontificia Comillas en el

curso académico 2021/2022 es de mi autoría, original e inédito y

no ha sido presentado con anterioridad a otros efectos.

El Proyecto no es plagio de otro, ni total ni parcialmente y la información que ha sido tomada de otros documentos está debidamente referenciada.

Fdo.: Claudia Vázquez Sanz

Fecha: 14/ 07/ 2022



Autorizada la entrega del proyecto

EL DIRECTOR DEL PROYECTO

Francisco J.
Lopez-Valdes

Firmado digitalmente
por Francisco J. Lopez-
Valdes

Fecha: 2022.07.15
16:42:47 +02'00'

Ad astra per aspera!

Acknowledgements

I would like to dedicate the present Master Thesis to all of those who, directly or indirectly, supported me within the last two years, which have not been the easiest due to the sanitary conditions. Thank you very much for keeping an eye on me and helping me to become the accomplished engineer that I am today. However, I would like to have some special words for the following:

First of all, I want to thank my parents for bringing me the opportunity of pursuing my master's degree in Madrid and especially at Pontifical Comillas University (ICAI). Thanks for being parents 24h a day, and thanks for trusting me and never letting me down in every single step I took in these last two years.

Next, I would like to thank my principal instructor, Francisco J. López Valdés, for giving me the chance of being part of the ICAI community and for choosing me to participate in this exciting research project. Thank you, Fran, for always keeping an eye on me and helping me and my colleagues every single time we needed it. Never stop wearing that smile and never change your cheerful personality, because, at the end of the day, that is what is truly valued by your peers.

Moreover, I would like to dedicate this project to my second instructor, Elena M. Tejado Garrido, from the Technical University of Madrid (UPM), who was also my Bachelor Thesis principal instructor when I finished my bachelor's degree in Materials Science and Engineering. Thank you very much for assisting me once again in all the testing stages that I performed at UPM's materials science department, for sharing all your knowledge with me and for always being down to help with a smile on your face.

Additionally, I want to dedicate this research project to my colleague Ignacio Victoria Rodríguez, who also worked on it with me and without whom all of these would have not been possible. Thanks for being there every single time I asked for help and for leading me in the laboratory when I started working on this study.

Special thanks as well to Eva Paz Jiménez and Juan Manuel Asensio Gil, who taught me how to use the optical microscope, and to Susana Guzmán, who was always available to help in the laboratory if needed. Thank you for all the knowledge and for being that close and nice to me.

Also big thanks to Sandra Tarancón, from Technical University of Madrid, who once again received me with open arms and was there throughout every single testing stage of the project to help.

And lastly, I would like to acknowledge every single person who works at ICAI's and UPM's materials science labs, because at the end of the day, I spent lots of hours of these last two years at these schools' facilities, always learning and acquiring new ski

Abstract

This project aims to gain insight into the mechanical and compositional properties of growing cortical bone tissue to improve the knowledge of juvenile bone to cope with the existing practical difficulties of testing human pediatric tissue.

Coupons from two different animal species (bovine and ovine) were made out of cortical areas of long bones to understand how mechanical and chemical properties vary within specimens of three different developmental stages: breastfed, solid-food-transitioning and mature. Once the bone samples were fabricated, they were subjected to tensile tests and nanoindentation analysis in order to determine mechanical properties such as maximum strength, maximum stress and elastic modulus, respectively. Tensile tests were recorded with a high-resolution camera to perform digital imaging correlation analysis and obtain the strain maps and strain values to which the bone coupons were subjected to.

Moreover, Scanning Electron Microscopy (SEM) and Energy Dispersive X-ray analyses were performed to observe the surface fracture of the specimens, as well as to determine the chemical composition of the samples and how it varied with age, respectively. Bone coupon surface exploration revealed that most of them experienced brittle fracture behaviour, besides an ovine sample which showed small plastic deformation signs. These statements were confirmed by analyzing the stress-strain curves.

From the experimental campaign, it has been concluded that juvenile bone tissue becomes stiffer and more resistant to fracture with age. In addition, it has been addressed that the calcium mass percentage, and therefore the tissue's mineralization grade, grew with increasing age, positively correlating with elastic modulus and bone strength. Furthermore, it has been possible to establish a common trend across species, since both bovine and ovine bone tissues behaved practically in an identical way.

Resumen

La finalidad de este proyecto es profundizar en el comportamiento mecánico y en las propiedades químicas de tejido óseo cortical de distintas especies animales en etapas tempranas de desarrollo, para tratar de ampliar el conocimiento actual en materia de dicho tejido y poder proponer así, soluciones a las dificultades existentes hoy en día a la hora de trabajar con dichos tejidos en sujetos pediátricos.

Para ello, se fabricaron probetas de hueso cortical procedentes de huesos largos de especies bovinas y ovinas que se encontraban en diferentes etapas de desarrollo: animales que estaban en la etapa de amamantar, aquéllos que se encontraban en el período de transición de amamantar a pienso o pasto y animales cuya dieta se basaba ya en alimentos sólidos. Una vez fabricadas, éstas fueron sometidas a ensayos de tracción y de nanoindentación para determinar propiedades mecánicas tales como fuerza y tensión máxima, o el módulo elástico, respectivamente. Los ensayos de tracción fueron grabados con una cámara de alta resolución para posteriormente realizar un estudio de correlación digital de imágenes y obtener así los mapas de deformación y los valores de dicho parámetro que experimentaron las muestras ensayadas.

Adicionalmente, se llevó a cabo un estudio fractográfico con el Microscopio Electrónico de Barrido (SEM) para analizar la superficie de fractura de las muestras. Dicho estudio reveló que la mayoría de las muestras experimentaron un comportamiento a rotura frágil, exceptuando la única muestra de origen ovino ensayada, que mostró indicios de deformación plástica. La anterior afirmación fue además corroborada con las curvas de tensión-deformación de los ensayos. Por otro lado, también se realizó un análisis composicional de las muestras mediante Espectroscopía de Dispersión de Rayos-X (EDX) para determinar su composición química y cómo ésta varía con la edad.

Tras la realización de los ensayos, se ha demostrado que el tejido óseo joven tiende a hacerse más resistente y rigidizarse con la edad. Además, se ha comprobado que el contenido en calcio aumenta con la edad, estando directamente relacionado con el incremento de módulo elástico y de resistencia mecánica del hueso. Observando todos los resultados, ha sido posible establecer la existencia de una tendencia común entre ambas especies analizadas, pues los tejidos de iguales etapas de desarrollo se comportaron de manera muy similar.

Index

1. Introduction	1
2. Objectives.....	3
3. Sustainable Development Goals (SDG)	4
4. Materials and Methods	5
5. Results and Discussion	12
5.1 Tensile Testing and Digital Imaging Correlation (DIC).....	12
5.2 Fractographic Analysis	16
5.3 Nanoindentation tests	20
5.4 Compositional Analysis	24
6. Conclusions.....	29
6.1 Future work.....	30
7. References.....	31

Figure Index

Figure 1. Typical bone structure, distinguishing between cortical and trabecular bone.	2
Figure 2. Coupon geometry used for mechanical tests.....	5
Figure 3. Micromet cutting tool (left) and Optimum milling machine (right) used for coupons fabrication.....	5
Figure 4. High-resolution Olympus digital microscope used for performing preliminary imaging.	7
Figure 5. Testing setup (camera and tensile test machine, left picture) and clamping system (right picture) used for tensile tests.....	8
Figure 6. Zeiss Auriga Gemini Scanning Electron Microscope used for fractographic and compositional analysis.....	9
Figure 7. Nano Indenter XP is used for performing nanoindentation tests.....	11
Figure 8. Coupons' head defects that have been detected through digital imaging microscopy. These may have surged during the fabrication process or as a result of already existing bone irregularities.	12
Figure 9. Stress vs strain curves of the bone coupons that broke in the cane area.	14
Figure 10. Tensile strain results based on digital imaging correlation for O3.5 sample.	15
Figure 11. SEM fractographies of V1.3 (top) and V1.4 (bottom) surface fractures. Both samples showed a brittle fracture behavior.	16
Figure 12. SEM fractographies of V2.2 (top) and V3.2 (bottom) surface fractures. As in the previous cases, it is clear to see that the coupons experienced a brittle fracture behavior.....	17
Figure 13. SEM fractographies of O3.5. Unlike the previous, this fracture shows signs of microdeformation, which are an indicative that the sample had an elasto-plastic behavior.....	18
Figure 14. SEM fractographies of O2.1 (left) and O3.1 (right) surface fractures. Compared to bovine specimens, it is possible to address that ovine samples show more pores throughout their respective cross sections.....	19

Figure 15. Optical microscopy image of 5 isolated indentations at a depth of 500 nm. The distance between each indentation was 25 μm 20

Figure 16. Optical microscopy image of 5 isolated indentations at a depth of 2000 nm. The distance between each indentation was 25 μm 20

Figure 17. SEM image of 5 isolated indentations at a depth of 2000nm. The distance between each indentation was 25 μm 21

Figure 18. Representative load-displacement indentation curves for bone tissue..... 21

Figure 19. Bar chart representing the mean value of Young’s modulus (E) with the respective standard deviations for the analyzed samples. Bovine specimens are displayed with red-coloured bars, while ovine specimens are represented in blue. SFT refers to solid-food-transitioning specimens. 23

Figure 20. Compositional spectrum of O3.5 sample surface fracture obtained using EDX technique..... 24

Figure 21. Calcium mass percentages reported with EDX analysis with their respective standard deviations. Bovine specimens are displayed with red-coloured bars, while ovine specimens are represented in blue. SFT refers to solid-food-transitioning specimens. 27

Table Index

Table 1. Samples geometrical measurements.	6
Table 2. Mechanical properties determined from the tensile test of the five samples that broke in the cane.	14
Table 3. Nanoindentation analysis results.	22
Table 4. Compositional analysis results obtained for eighteen samples using EDX. Results are displayed with its respective standard deviations.	26

1. Introduction

Bone is a heterogeneous, anisotropic natural composite material consisting of collagen fibrils (30-40 weight %), a mineral phase (50-60 weight %) and water (10-20 weight %). The bone structure has evolved to bear physiological loads, being able to partially tune its mechanical properties through remodelling. Although multiple factors contribute to their structural integrity: the total bone mass, bone geometry, microdamage and microstructural discontinuities (such as microporosity) and the properties of the constituent tissue. Changes in each of the constituents may have significant effects on the fragility of the bone. Among them, the mineral phase, with greater elastic modulus, provides rigidity to the bone and makes it behave anisotropically due to the uneven distribution of the crystal minerals [1]. Additionally, recent studies have found that the collagen phase may also play a significant role in the mechanical behaviour of bones: the mineral component predominantly contributes to bone stiffness, whereas the the quality of the collagen phase plays an important role when determining the toughness of bone tissue[2].

On the other hand, the mechanical behaviour of the bone tissue is also influenced by age, genetic or metabolic diseases, as well as environmental conditions, which may increase the risk of fracture and affect its mechanical integrity. After reaching peak bone mass in the third or fourth decade of life, both the quantity and quality of bone tissue in the human skeleton begin to deteriorate.

Ageing is associated with changes to the bone structure at small and large length scales that deteriorate its strength (that is, intrinsic resistance) and toughness (that is, extrinsic resistance), respectively [3]. It has been reported that ageing has significant effects on the mechanical properties of the collagen phase in cortical bone [1]. Cortical bone is a dense mineralized tissue that encloses trabecular bone in epiphyses and is also found in the diaphysis of long bones [4]. It exhibits a complex hierarchical structure that confers high strength and toughness properties, which lead to intrinsic plasticity-based mechanisms at small length scales and extrinsic crack-shielding mechanisms at larger length scales [3].

Since the bone is a hierarchical bio-composite material made of an organic matrix (collagen type I fibrils) filled with a mineral component consisting of apatite crystals that interact with these collagen fibrils, its mineral content plays a major role in the bone strength. However, there are very little data on the characterization of healthy juvenile bone at the tissue level [5], so the fact of obtaining information on that would help to explore alternative methods to scale material properties for different ages.

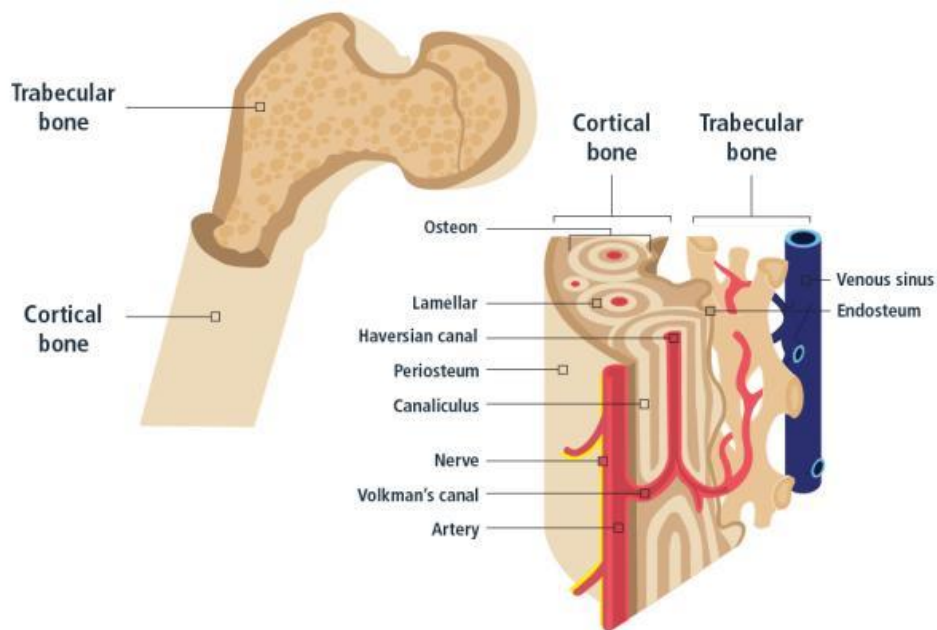


Figure 1. Typical bone structure, distinguishing between cortical and trabecular bone.

In this study, bone coupons from two different animal species (bovine and ovine) were made out from cortical areas of long bones to compare how bones' mechanical properties vary at different juvenile developmental stages of the tissue.

Mechanical testing allows direct assessment of a range of mechanical properties across multiple length scales, allowing characterization of multiple structural and material properties. At the macroscopic level, whole-bone testing allows the assessment of bone structural properties such as stiffness and strength.

At smaller length scales, material testing techniques enable measurement of the intrinsic properties of the tissue such as elastic modulus and ultimate stress [6]. Moreover, the assessment of tissue composition (both inorganic and organic components) should be addressed since it directly contributes to the structural integrity of the whole bone. Consequently, a chemical and compositional analysis was parallelly carried out on the samples to quantitatively check how its composition differs with age.

Therefore, the aim of this research project is to quantify whether the change in mechanical properties at different developmental stages is related to the change in bone tissue composition in a similar fashion across species.

2. Objectives

As a consequence of the aforementioned, this research project aims to quantify whether the change in mechanical properties at different juvenile developmental stages is related to the change in bone tissue composition in a similar trend across species. More specifically, the project steps can be summarised as follows:

- Mechanical characterization of the bone coupons by performing tensile tests to determine the maximum strength, maximum stress, Young's modulus, and deformation experienced by each of the evaluated samples. A preliminary visual inspection was also performed prior to tensile tests to detect surface fabrication defects.
- Nanoindentation analysis on bone prepared samples to obtain accurate Young's modulus values (since not all the specimens broke in the narrower area and results from the stress-strain curve may not be accurate enough).
- Fractographic analysis using a Scanning Electron Microscope (SEM) was carried out to obtain information regarding the micro-mechanisms of failure involved and its correlation with the macroscopic fracture behaviour. Moreover, this equipment was also used to perform Energy Dispersive X-Ray Analysis (EDX) to identify the elemental composition of materials, and to study how bone compositions change with age in the analyzed species.
- With all the gathered data, relate how changes in composition influences bone behavior at different developmental stages.

3. Sustainable Development Goals (SDG)

The Sustainable Development Goals (SDGs) are the world's shared plan to end extreme poverty, reduce inequality and protect the planet by 2030. They emerged from the most inclusive and comprehensive negotiations in the United Nations (UN) and they have been adopted by 193 countries in 2015. The UN Foundation focuses on ideas and initiatives that generate a larger impact, advance the SDG imperative to leave no one behind, and are backed by evidence, practical commitments, and action.

Particularly, this project lines up with SDG number 3, "Good Health and Well-Being", which focuses, within other objectives, on mitigating the new-born and under 5 years old children's avoidable deaths, ensuring that all countries try to reduce new-born mortality to at least 12 per 1000 live births, and under-5 mortality to at least 25 per 1000 live births. The research study aims to understand how mechanical properties and composition of bone tissue vary with age, being the final goal to try to extrapolate these results to humans to develop a children's injury criterion for road accidents.

Moreover, SDG number 9 "Industry, Innovation and Infrastructure" aligns with the current research project, since once the conclusions are confirmed, the foundation for exploring alternative methods to scale material properties for different ages based on more extensive animal tissue (that can easily include juvenile tissue as a way to cope with the existing practical difficulties of testing human pediatric tissue) will be stated, contributing to innovation and testing easiness.

4. Materials and Methods

Long bones (tibias and femurs) of two mammal species (bovine and ovine) were sourced from local providers ensuring (through source tracking) that the bones were within the appropriate age groups: breastfed, solid-food-transitioning, and mature (employing nutrition as a proxy for age). Breastfed species include cows until 12 months of age and sheep until 4 months; solid-food-transitioning will be those starting to graze, and it will cover bovine species between 12 and 18 months and ovine species on a range from 4 to 12 months; while mature species will go from 18 months and 12 months onwards for cows and sheep, respectively. After cleaning (scraping the nutrient foramen away and removing the marrowbone), the diaphyseal areas were cut into sections perpendicular to their longitudinal axes. These sections were then machined into 0.8 mm longitudinal sheets of cortical tissue, employing a refrigerated circular diamond-encrusted blade (*Remet Micromet Evolution 8502, Bologna, Italy*) from which the final dog-bone coupons were cut out (6x2.5mm² stem), the average geometry of the specimens can be observed in Figure 2. The circular hollow areas were drilled using an *Optimum Maschinen BF 20 Vario (Germany, GmbH)* milling tool, which can be seen in Figure 3. Further details on the bone followed wafer machining process can be found in *Submit et al. [7]*.

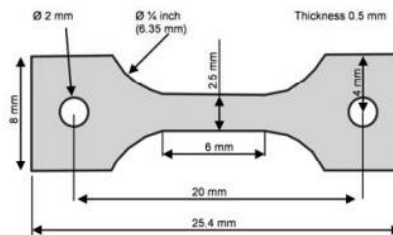


Figure 2. Coupon geometry used for mechanical tests.



Figure 3. Micromet cutting tool (left) and Optimum milling machine (right) used for coupons fabrication.

Twenty-six bone coupons were fabricated for this study. Specimens were classified into six different groups and six samples were made for each group (one for each age and species), except for group 6, where only two samples were included due to insufficient raw material. The fabricated coupons were then preserved refrigerated and in a NaCl solution (*VisClean Physiological Saline Solution, France*) to keep the samples hydrated throughout the process.

Table 1. Samples geometrical measurements.

Sample ID	Gage thickness (mm)	Gage Width (mm)	Gage Length (mm)	Cane Fracture?
V.1.2.T	0.74	2.40	6.20	No
V.1.3.T	0.65	2.37	6.35	Yes
V.1.4.T	0.81	2.42	6.05	Yes
V.1.5.T	-	-	-	Broke prior to testing
O.1.2.T	0.78	2.11	6.12	No
O.1.3.T	0.71	2.49	6.07	No
O.1.4.T	0.72	2.16	6.10	No
O.1.5.T	1.02	2.53	6.15	No
V.2.2.T	0.87	2.70	6.34	Yes
V.2.3.T	0.82	2.49	6.14	No
V.2.4.T	-	-	-	Broke prior to testing
V.2.5.T	0.79	3.42	6.06	No
V.3.2.T	0.83	2.47	6.11	Yes
V.3.3.T	-	-	-	Broke prior to testing
V.3.4.T	0.97	2.00	6.04	No
V.3.5.T	0.88	2.19	6.24	No
O.2.2.T	0.97	2.70	6.15	No
O.2.3.T	0.79	2.53	6.03	No
O.2.4.T	-	-	-	Broke prior to testing
O.2.5.T	-	-	-	Broke prior to testing
O.3.2.T	0.83	2.57	6.21	No
O.3.3.T	0.74	2.46	6.05	No
O.3.4.T	0.81	2.48	6.15	No
O.3.5.T	0.71	2.41	6.08	Yes
V.1.6.T	1.40	2.31	6.02	No
V.2.6.T	-	-	-	Broke prior to testing

Before testing, the sample surfaces were evaluated using digital microscopy imaging to detect possible defects that may lead to fracture on a determined area of the coupon. An *Olympus DSX10-UZH* High-Resolution Digital Microscope (*Tokyo, Japan*) equipped with a tilt frame system and telecentric lens, was used to perform the aforementioned surface inspection. This microscope, which can be seen in Figure 4, besides other multiple functionalities, allows to measure surface roughness, providing 3D plots which give information regarding the depth changes throughout a selected superficial area.



Figure 4. High-resolution Olympus digital microscope used for performing preliminary imaging.

Before starting the testing campaign, coupons were coated with a white primer and misted with black spray paint to generate a random speckle pattern; this procedure is needed to facilitate the digital imaging correlation (DIC) once the tests are done.

Coupons were then attached to an *Ibertest IBTH-5/500 (Spain)* tensile testing machine with an in-home specifically designed aluminium clamping system so that misalignment between the top and bottom ends of the coupons is avoided. Since the samples used in this study are pretty fragile, the installation of the coupons without applying such loads that could generate bending, shear, or excessive tension, is critical. Conventional fixed wedge clamps would not ensure the required control of the load during the installation of the coupons, so these were attached to the clamping system through tempered steel cylindrical pins, as can be seen in Figure 5.

The testing conditions followed ASTM Standard E 1012-99 [8], thus quasi-static tests were performed in these coupons at 50 mm/min pulling speed with a 2.2 N pre-load.

A *DTS (Diversified Technical Systems) Slice Ware (California, USA)* acquisition system was connected to the tensile testing machine, as well as to a high-speed *iXCamera*. The tensile testing machine load signal was triggered and tests were recorded with the aforementioned high-speed camera at 100 frames per second. After that, the videos were imported into the *GOM Correlate software (Zeiss, Germany)*, to track the point cloud deformation and estimate deformations in each of the analyzed samples.



Figure 5. Testing setup (camera and tensile test machine, left picture) and clamping system (right picture) used for tensile tests.

Additionally, fractographic and compositional analysis was performed to check the surface fracture topologies and to address how bone's composition varied with age, respectively. The coupons were examined using a Scanning Electron Microscope (SEM, Zeiss Auriga Gemini). This microscope, which can be seen in Figure 6, provides high-resolution and high-magnification images from the material's surface as a result of electrons' interaction with the sample. It is equipped with a filament that generates an electron beam to lighten the specimens. From the beam-surface interaction, electrons are generated and picked by multiple detectors which can create an image that reflects the surface topology, as well as geometric features and texture data [9].

Depending on the beam's interaction with the sample, it will be possible to capture diverse effects that we would visualize depending on the used equipment. Within those possible effects, the following can be distinguished:

- Secondary electrons (SE): very low energy electrons, below 5 eV, which are produced when an electron from the beam passes close to one of the sample's atom core. This provides enough energy to one or more electrons so they can jump out of the sample. Since these electrons have very low energy, they are located in the surface of the specimen so topographic information is obtained from them. Secondary electrons are the most used in scanning electron microscopy [9].
- Backscattered electrons: they are generated when a beam's electron frontally hits a sample's atom core, being repelled backwards. The aforementioned effect intensity varies proportionally with the atomic number. That is the reason why they are used to obtain specimens' superficial compositional maps.

- It is worth mentioning Auger electrons, which appear when a secondary electron is expelled from the atom and an outer electron jumps into the interior to fill the aforementioned gap. As a consequence, an energy excess appears and it is corrected with the emission of a new electron of the most external layer, the so-called Auger electrons. Likewise, the backscattered electrons, are used to obtain contrast compositional information about the sample, specifically of very small areas of the surface [9].
- X-Rays: in the aforementioned process, the excess energy can be balanced with X-ray emission as well. These are characteristic of each sample's element, so they are also used to obtain chemical compositional information [9].

The *Zeiss Auriga Gemini* is equipped with secondary electron detectors (SE), backscattered electron detectors (BSE), and X-ray dispersion detectors, which allow performing Energy Dispersive X-ray Analysis (EDX) to identify the elemental composition of materials. For the compositional analysis, *QUANTAX* software (*Bruker AXS*) was used. It is based on X-ray dispersive energy microanalysis (EDX) to automatically analyze the compositional elements of each of the samples.

For the fractographic study, the working voltage was 15 kV and only the surface fracture of coupons that broke in the cane was inspected.



Figure 6. Zeiss Auriga Gemini Scanning Electron Microscope used for fractographic and compositional analysis

Before their observation in the SEM, samples were required to be prepared. Since bones are non-conductive materials and the SEM working principle uses electrons to create the images, a metalizing process was applied to the specimens right before analyzing them. Firstly, they were mounted on conductive metallic holders by using a conductive carbon tape. After that, a 12.67 nm carbon layer was deposited in each of the samples using a *Leica EM ACE600* metallizer. Metalizing vacuum pressure was 10^{-4} mBar and 26 pulses were required to deposit the adequate conductive layer thickness.

Lastly, nanoindentation analysis was carried out on 18 samples to determine the elastic modulus of the different species and ages. Nanoindentation has been widely used in materials science, especially for assessing surface properties on thin films [10]. These advances have been made possible by the development of instruments that continuously measure force and displacement as the indentation is done, avoiding the limitations of optically measuring the imprints. The technique uses a diamond indenter to load and unload a material specimen leaving a permanent indent on the surface. The two mechanical properties measured most frequently using load and depth-sensing indentation are the elastic modulus E , and the hardness H . Data are obtained from one complete cycle of loading and unloading and analyzed according to a model for the deformation of an elastic half-space by a rigid, axisymmetric punch derived previously by Sneddon [11]. The mathematical solution was adapted for the nanoindenter geometry by Oliver and Pharr [12]. The stiffness S is related to the reduced modulus E_r by:

$$S = \frac{dP}{dh} = \beta \frac{2}{\sqrt{\pi}} E_r \sqrt{A} \quad (1)$$

Where A is the projected area of contact (a function of depth, h) and β is an empirical shape factor.

The reduced modulus, E_r , accounts for using a nonrigid indenter and is determined by the following equation:

$$\frac{1}{E_r} = \frac{(1 - \nu_s^2)}{E_s} + \frac{(1 - \nu_i^2)}{E_i} \quad (2)$$

Where E_s and ν_s are the sample modulus and Poisson's ratio and E_i and ν_i are the indenter modulus and Poisson's ratio.

The hardness of bone tissue can also be determined by

$$H = \frac{P_{max}}{A} \quad (3)$$

Where P_{max} is the peak indentation load and A is the projected contact area (tetrahedron including the rounding of the tip) at that load.

These tests have been conducted on cortical bone samples using an *XP Nano Indenter (MTS)*, which can be seen in the image below, equipped with a *Berkovich* diamond tip, and following the Oliver and Pharr [12] methodology.

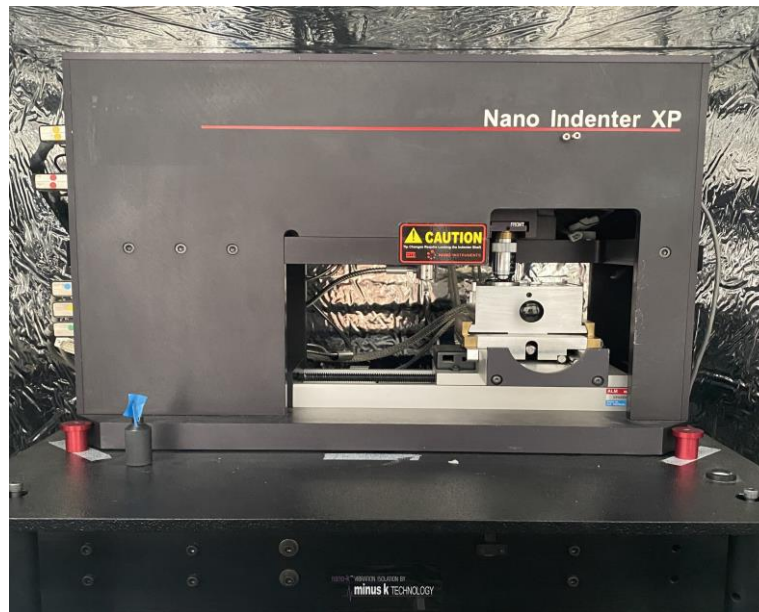


Figure 7. Nano Indenter XP is used for performing nanoindentation tests.

Before the indentation process, samples should be accurately polished so that the surface does not exhibit irregularities that may influence the results. Bone coupons were cut into smaller pieces with a *Walter EBNER (Well, Le Locle)* diamond wire saw to embed them in an epoxy resin (*Mecaprex MA2+, Presi*). Once the resin was cured, the mounted specimens were polished using an *ABRAMIN Struers (Germany)* polisher. Different silicon carbide sandpaper rugosities (400, 600, and 1200 grit) were used until the desired surface finish was achieved.

Finally, each sample was indented with a 10x5 array and a 25 μm distance was set between each indentation to avoid interaction between each indent. Load control tests were performed up to 5mN, which resulted in a penetration depth of 500 nm. A 0.3 Poisson's modulus was considered in this study [10], [13], is consistent with recently reported values for human femoral cortical bone (0.28).

5. Results and Discussion

5.1 Tensile Testing and Digital Imaging Correlation (DIC)

Tensile tests have been conducted to determine maximum strength, maximum stress, and deformation of the bone coupons. Twenty samples were used for this testing stage. It is important to note that coupons have been named based on animals' feeding developmental stage and the group to which they belong. V1 and O1 will be used to refer to breastfed species (bovine and ovine, respectively), V2 and O2 to solid-food-transitioning, and V3 and O3 to refer to mature mammals. For example, sample V1.2 refers to a breastfed bovine bone coupon and belongs to group 2. Note that samples from group one have not been considered for this analysis, since they have been previously tested with a completely different setup.

Only five samples broke in the cane area (narrower part), whereas the other experienced fracture in the joint to the clevis pins. The latter may be a result of misalignment of samples' drills which concentrate the stress away from the middle or because of the stress concentrations that appear due to the contact area between the cylindrical pins that have been used for the clamping system in the coupon's heads. Moreover, some defects were detected in the aforementioned locations when performing preliminary digital microscopy imaging, so those could have also led to fractures in those points, as it can be seen in Figure 8. However, regarding the maximum strength results displayed in Table 2 (which includes the maximum strength exhibited by each sample, as well as the maximum stress and maximum strain values for the samples that broke in the cane), it is possible to note that some of the coupons that did not broke in the cane withstood even higher loads than those which experienced fracture in that area. Those results were not taken into account for this study, since that samples did not broke in the cane area, thus they would not be representative of the mechanical properties of the material. Nevertheless, the fact that they bore such loads is an indicative that the gage was able to withstood the fracture load, so in future experiments, it will be interesting to fabricate samples with lower gage width so that the fracture will be more likely to happen in that area.

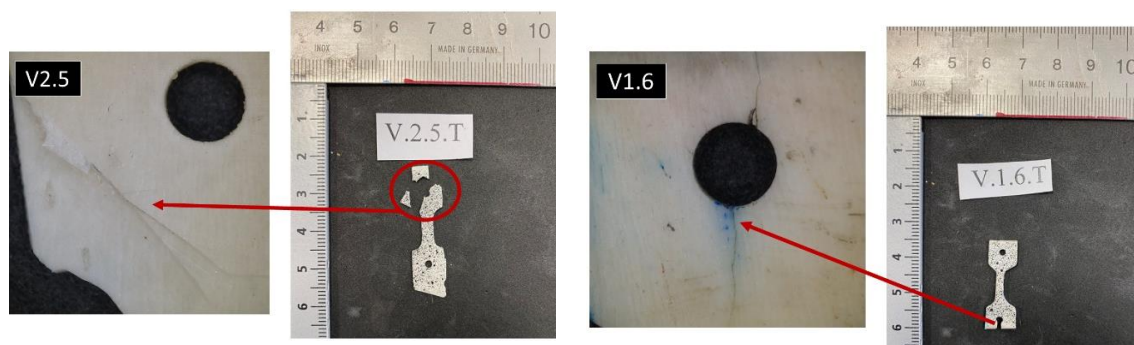


Figure 8. Coupons' head defects that have been detected through digital imaging microscopy. These may have surged during the fabrication process or as a result of already existing bone irregularities.

Stress vs. strain curves were plotted for each of the samples that broke in the cane. Stress was calculated as the tensile force divided by the initial cross-section in the middle of the gage area, using the following equation:

$$\sigma = \frac{F}{A} \quad (4)$$

Where σ is the resulting stress, F is the applied tensile load and A is the coupon's cross-section measured in the middle of the cane area.

On the other hand, the strain was calculated using the displacement measurements provided by the tensile test machine, since the virtual extensometer strain analysis performed with *GOM Correlate* software did not provide the expected results. This was probably due to a lack of enough image resolution, therefore leading to unsuccessful software performance and the inability to correctly track the point cloud displacements.

The strain was calculated using the following equation:

$$\varepsilon = \frac{\Delta l}{l_0} \quad (5)$$

Where ε is the resulting engineering strain, Δl is the difference between the final and the initial length, and l_0 the initial gauge length (considering 20mm as the initial length, being the distance between the aluminium rods' drills to be consistent with the tensile testing machine results).

Stress vs strain curves are displayed in Figure 9. This is complemented with the results included in Table 2. Regarding these numbers, it can be seen that both stress and strength increased with age, reaching the former parameter values of 29.95 MPa and 25.85 MPa for breastfed samples, around 35 MPa for the solid-food transitioning bovine bone coupon, and 42.54 MPa and 90.5 MPa for mature bovine and ovine samples, respectively. The latter is an unusually high value since the coupon experienced signs of plastic deformation, which can be confirmed by its stress-strain curve shape, displayed in purple in Figure 9. As it can be seen, from approximately a strain value of 0.03, the curve stops being linear and slightly acquires the typical curve shape of the plastic deformation region. The other coupons showed a linear elastic behaviour up to fracture, probably leading to a brittle fracture behaviour, which will be confirmed with the fractographic analysis.

Elastic modulus results were not determined using these curves. Nevertheless, this material property was determined for a large number of samples via nanoindentation tests.

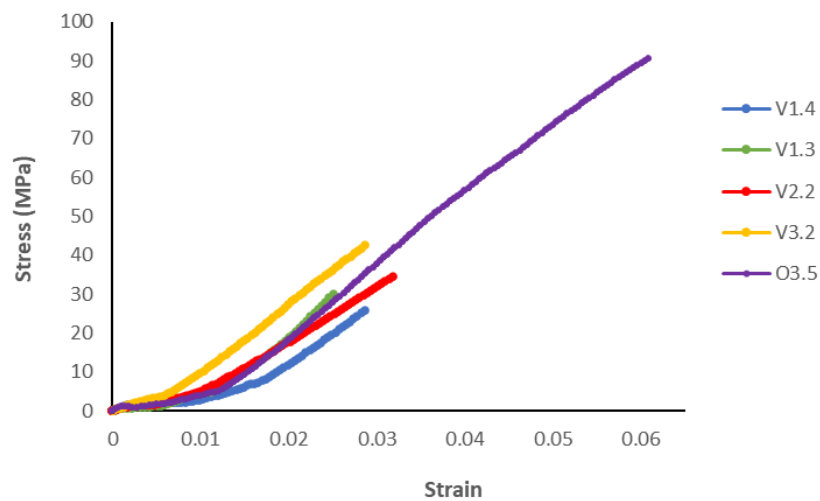


Figure 9. Stress vs strain curves of the bone coupons that broke in the cane area.

Table 2. Mechanical properties determined from the tensile test of the five samples that broke in the cane.

Sample ID	Maximum Strength (N)	Maximum Stress (MPa)	Maximum Strain
V.1.2.T	60.04	-	-
V.1.3.T	46.35	29.95	0.0261
V.1.4.T	50.43	25.85	0.0296
O.1.2.T	52.05	-	-
O.1.3.T	105.59	-	-
O.1.4.T	40.31	-	-
O.1.5.T	126.48	-	-
V.2.2.T	81.43	34.66	0.0327
V.2.3.T	171.98	-	-
V.2.5.T	224.82	-	-
V.3.2.T	87.21	42.5	0.0296
V.3.4.T	58.18	-	-
V.3.5.T	-	-	-
O.2.2.T	31.49	-	-
O.2.3.T	84.78	-	-
O.3.2.T	118.43	-	-
O.3.3.T	194.04	-	-
O.3.4.T	91.08	-	-
O.3.5.T	154.85	90.5	0.062
V.1.6.T	25.58	-	-

The mechanical properties of bone tissue change during growth. Bone becomes stiffer and more resistant to fracture [5]. This statement can be confirmed by the previous results, in which both strength and stress increased with age for the bovine specimens. Regarding the ovine samples, no conclusion can be placed since only of these samples broke in the cane area.

Additionally, deformation maps obtained with *GOM Correlate* software have been included, as proof that the higher strain values in the Y axis are present in the location in which the cane fractured. As it can be seen at the bottom of Figure 10, there are missing elements on the mesh, which are derived from the impossibility of the software to track the whole point cloud throughout the process; this may happen, especially when changes in the lighting or considerably large deformation are observed.

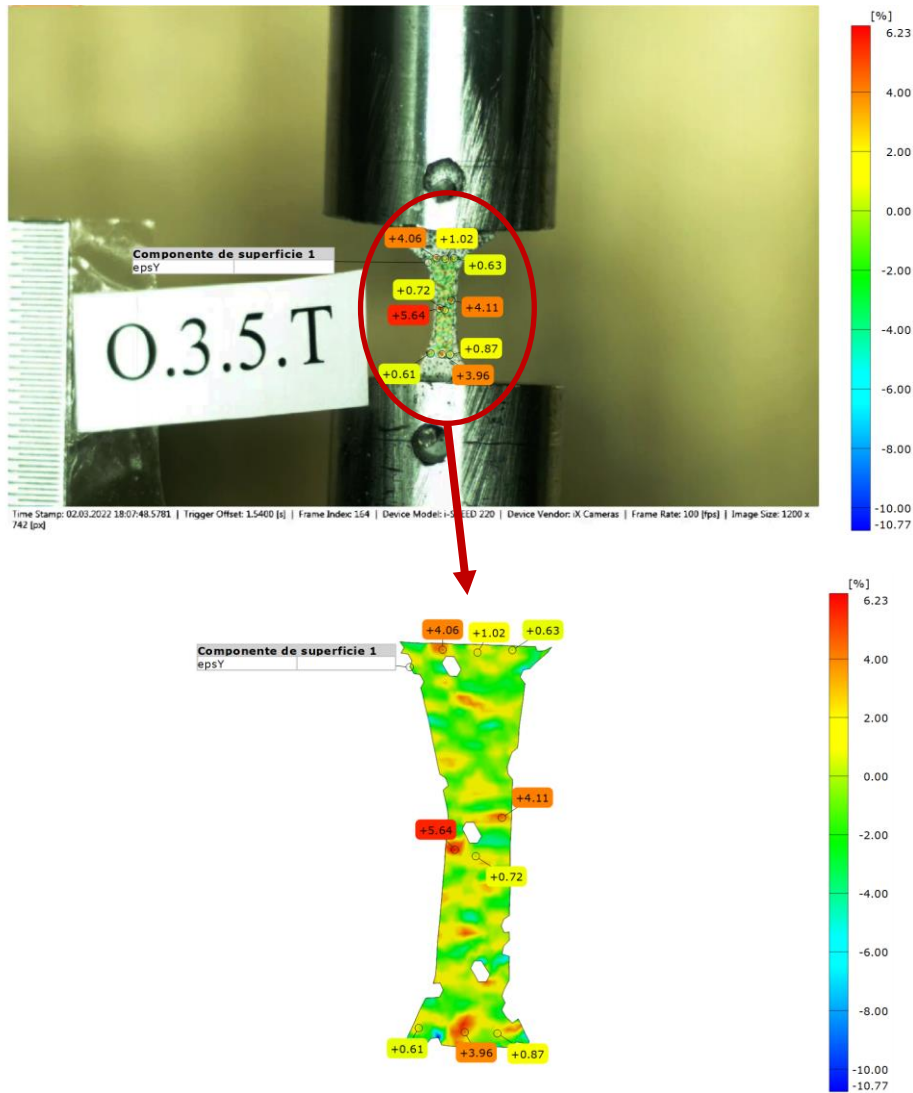


Figure 10. Tensile strain results based on digital imaging correlation for O3.5 sample.

5.2 Fractographic Analysis

The Scanning Electron Microscope, whose working principle has been already detailed in the previous paragraphs, was used to carry out this study. Each of the following images belongs to the surface fracture of the coupons that broke in the cane area. Secondary Electrons (SE) detectors were used to capture them.

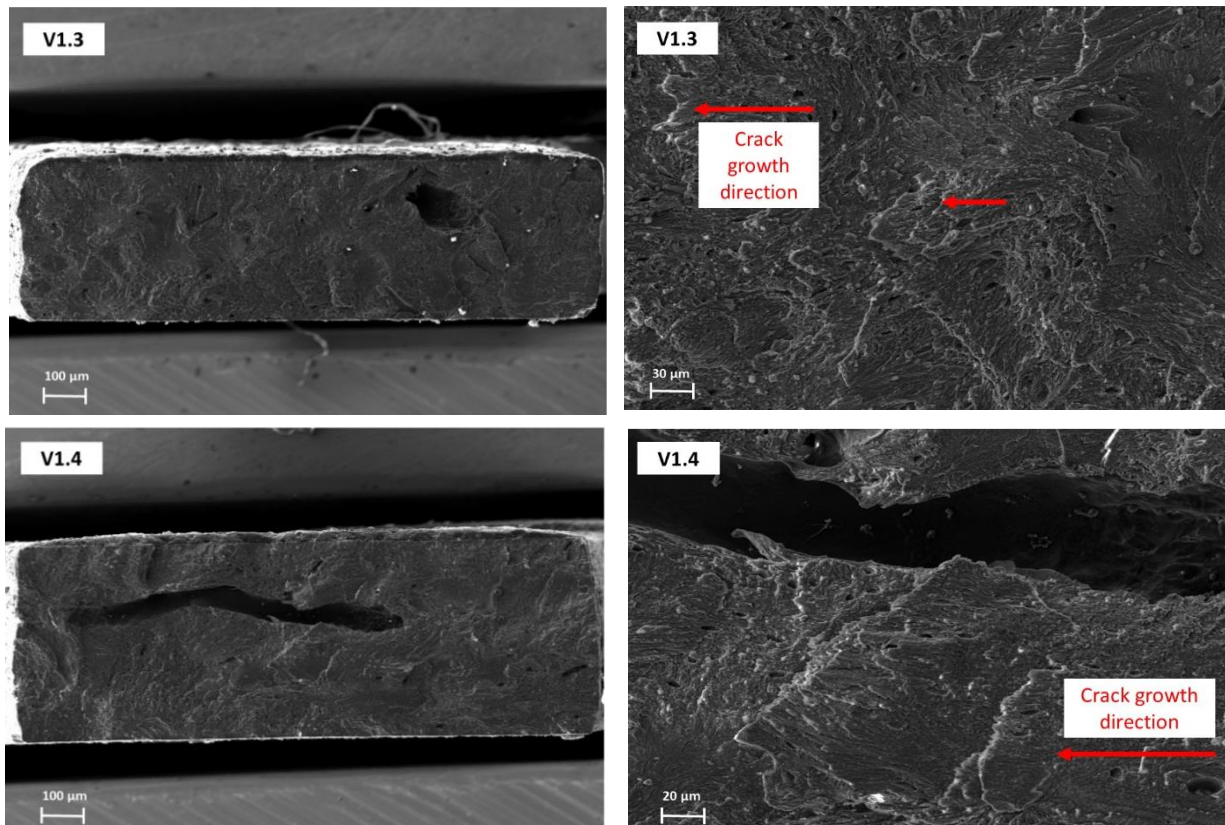


Figure 11. SEM fractographies of V1.3 (top) and V1.4 (bottom) surface fractures. Both samples showed a brittle fracture behavior.

Figure 11 shows micrographs at different magnification of two breastfed bovine samples. It is possible to observe that the surface fracture in both cases is very flat, which is indicative of a brittle fracture behaviour. Brittle fracture involves fractures without any appreciable plastic deformation and low energy release, which can be confirmed by the cleanliness of the surface, as well as with the stress curves in Figure 9, which showed a clear elastic behaviour up to fracture. Regarding the coupons' surface fractures more in detail, it is possible to observe that V1.3 has a pore on its right side. Pores are stress concentrators, so there is a high probability that the fracture was initiated at that location. Moreover, the fracture planes point towards the left, which indicates that the crack began at the right side of the surface, probably influenced by the pore presence. On the other hand, the V1.4 coupon's fracture seems not to have been mainly caused by its large pore.

By observing the orientation of the fracture planes, it is possible to determine that the fracture began on the right side of the sample. Regardless of that, the pore's dimensions are such that may have also contributed to fracturing.

Some features can be classified as micro deformation areas, but as in V1.3, the surface's pattern points out that the fracture has been macroscopically brittle.

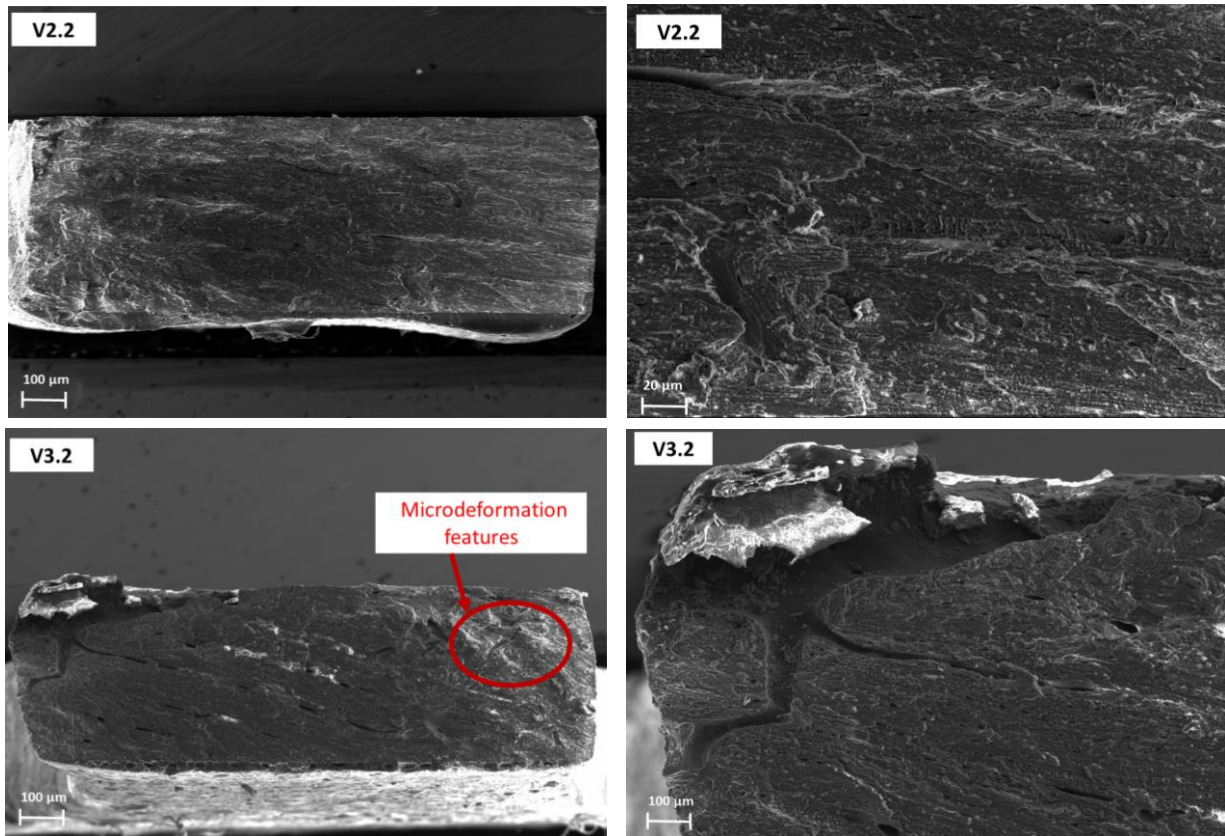


Figure 12. SEM fractographies of V2.2 (top) and V3.2 (bottom) surface fractures. As in the previous cases, it is clear to see that the coupons experienced a brittle fracture behavior.

Likewise in the breastfed samples fractography, those included in Figure 12 show the same fracture modes. The top images belong to a solid-food-transitioning bovine specimen, while those placed at the bottom come from a mature one. Regarding the first, it is clear to see that the fracture was pretty clean. Performing a higher magnification analysis, it is possible to observe that the fracture was initiated on the right side of the surface and that it came across some obstacles while moving forward since there are bone surface areas that lay at different heights. V3.2 surface fracture reveals once again a brittle behaviour. The crack is probably initiated at the left corner since under it there is a flat area and the planes' orientation points towards the right side of the surface. Moreover, multiple pores are as well oriented towards that side, but those may be an intrinsic feature of the bone. Additionally, there is an area in the right part of the sample that shows signs of micro deformation, but the fracture was macroscopically brittle.

Lastly, Figure 13 shows multiple fractographies of an ovine mature sample. This coupon was the one that withstood a higher load and as it can be seen in the images below, it shows large signs of micro deformation. Multiple fracture planes were observed, which is an indicator of the difficulties to advance of the crack to grow and, presumably, of the high fracture toughness of this material.

It is worth mentioning that ovine bone coupons are more porous than those coming from cows. This can be confirmed with the fractographic images shown in Figure 14. These samples belong to group one and they have been tested with a completely different tensile testing setup, which used conventional wedge clamps. The latter would not ensure the required control of the load during the installation of the coupon. However, a fractographic analysis was performed on them as well.

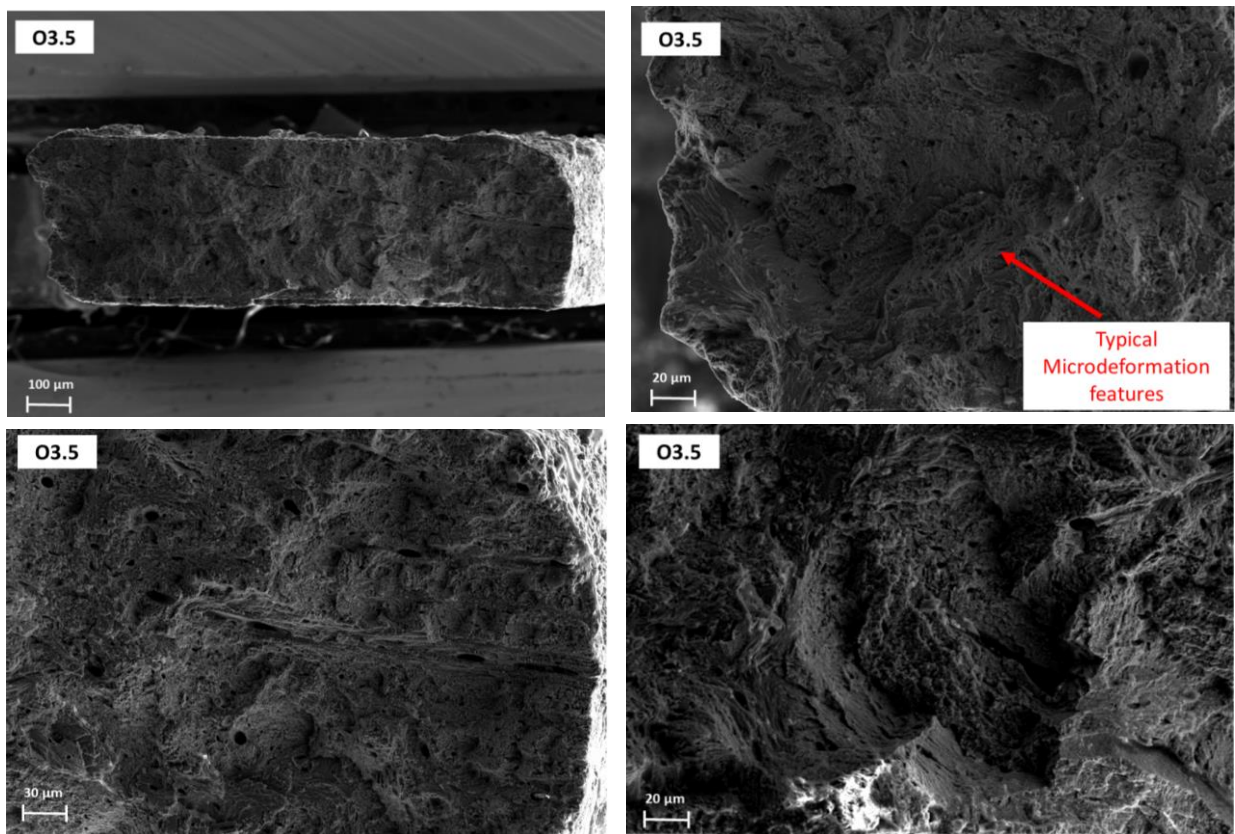


Figure 13. SEM fractographies of O3.5. Unlike the previous, this fracture shows signs of microdeformation, which are an indicative that the sample had an elasto-plastic behavior.

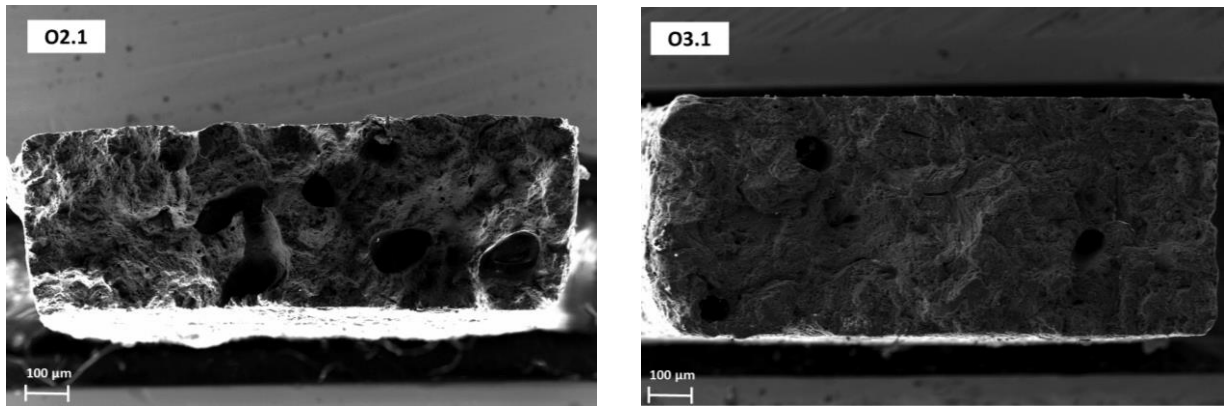


Figure 14. SEM fractographies of O2.1 (left) and O3.1 (right) surface fractures. Compared to bovine specimens, it is possible to address that ovine samples show more pores throughout their respective cross sections.

5.3 Nanoindentation tests

Nanoindentation testing has become a popular technique for addressing the mechanical properties of mineralized biological tissues, including bone or calcified cartilage. Due to the small volume of material sampled for each indentation test, the technique is well suited to the examination of local mechanical properties in inhomogeneous biological tissues [14]. The imprints left by the nanoindenter after testing the bone specimens can be appreciated in the following figures:

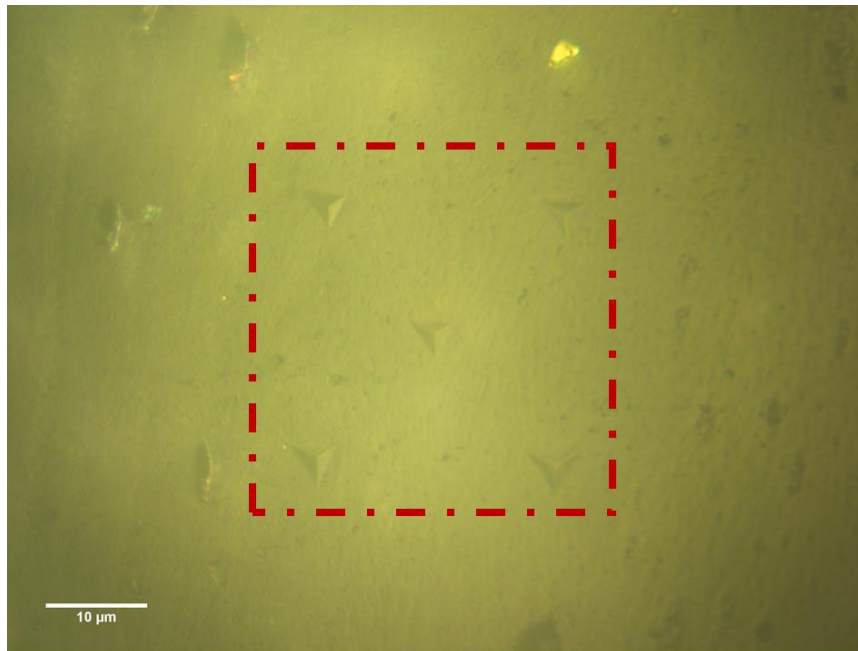


Figure 15. Optical microscopy image of 5 isolated indentations at a depth of 500 nm. The distance between each indentation was 25 μm .

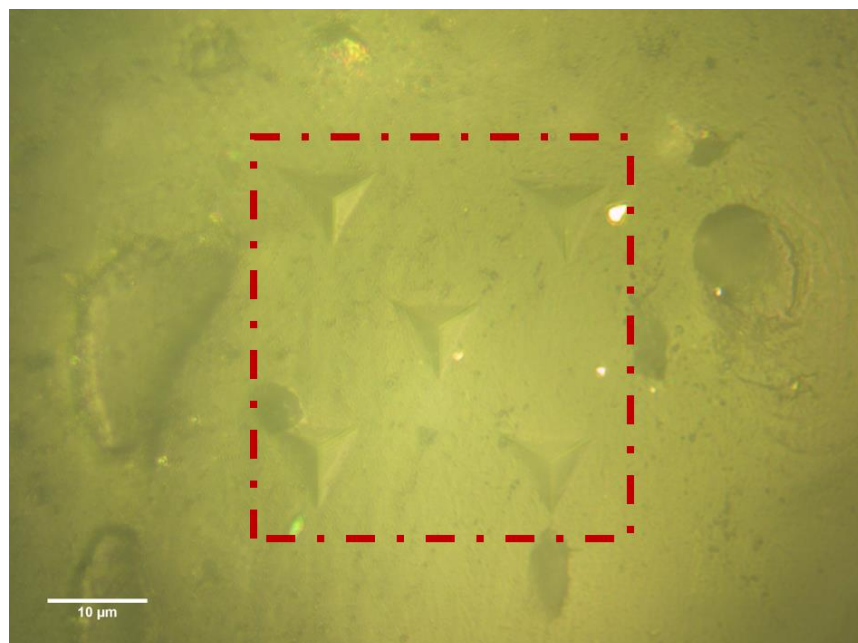


Figure 16. Optical microscopy image of 5 isolated indentations at a depth of 2000 nm. The distance between each indentation was 25 μm .

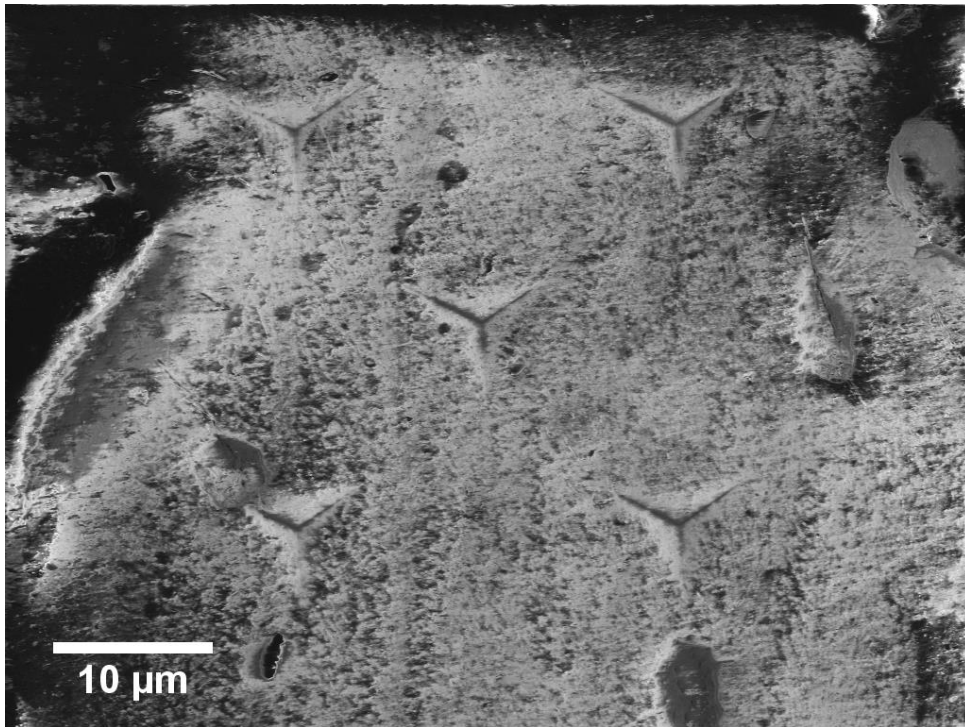


Figure 17. SEM image of 5 isolated indentations at a depth of 2000nm. The distance between each indentation was 25 μm.

The load and displacement curves depicted below represent the typical response to our samples during indentation tests. Elastic modulus was calculated from the slope of the initial segment (50%) of the unloading curve. Besides, hardness is computed from the maximum load, although this analysis is out of the scope of this research project.

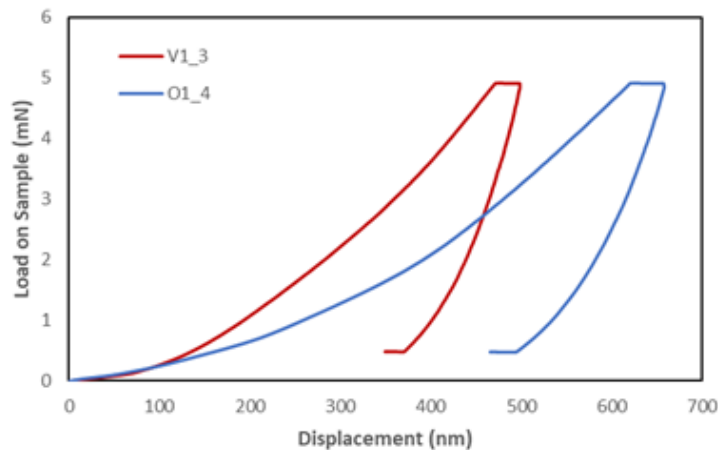


Figure 18. Representative load-displacement indentation curves for bone tissue.

The mean values and standard deviations of the elastic modulus of the analyzed samples are reported in Figure 19. A total of 18 samples were analyzed in this testing stage, being the results displayed in Table 3.

Table 3. Nanoindentation analysis results.

Sample ID	Species	E (GPa)
V1.3	Breastfed Bovine	18.43±1.61
V1.4	Breastfed Bovine	15.66±1.46
V1.5	Breastfed Bovine	22.13±2.94
V2.3	SFT Bovine	20.76±3.43
V2.4	SFT Bovine	22.29±1.06
V2.5	SFT Bovine	20.20±3.46
V3.3	Mature Bovine	21.11±2.59
V3.4	Mature Bovine	22.51±1.89
V3.5	Mature Bovine	20.91±2.09
O1.3	Breastfed Ovine	16.36±2.25
O1.4	Breastfed Ovine	14.31±2.32
O1.5	Breastfed Ovine	21.55±3.95
O2.3	SFT Ovine	17.72±2.99
O2.4	SFT Ovine	14.37±2.57
O2.5	SFT Ovine	18.65±3.17
O3.3	Mature Ovine	18.99±4.21
O3.4	Mature Ovine	16.73±3.81
O3.5	Mature Ovine	19.81±4.10

Results of three samples are included for each bar and, as mentioned before, 50 indents (matrices of 5x10) were performed on each of the bone specimens to obtain representative values of the overall behaviour of each material.

Mean numerical values of the elastic modulus for bovine breastfed bones are 18.7 ± 2 GPa, around 21.1 ± 2 GPa for solid-food-transitioning animals (SFT), and 21.5 ± 2.6 GPa for mature specimens. Regarding the values for the ovine specimens, those are 17.4 ± 2.8 GPa for breastfed animals, 17 ± 3 GPa for solid food transitioning, and of around 18.5 ± 4 GPa for mature bones.

The current nanoindentation measurements are consistent with other macroscopic and microscopic measurements for cortical bone. Literature values for cortical bone range relay between 17 and 20 GPa, depending on age and general tissue condition [7], [10], [15].

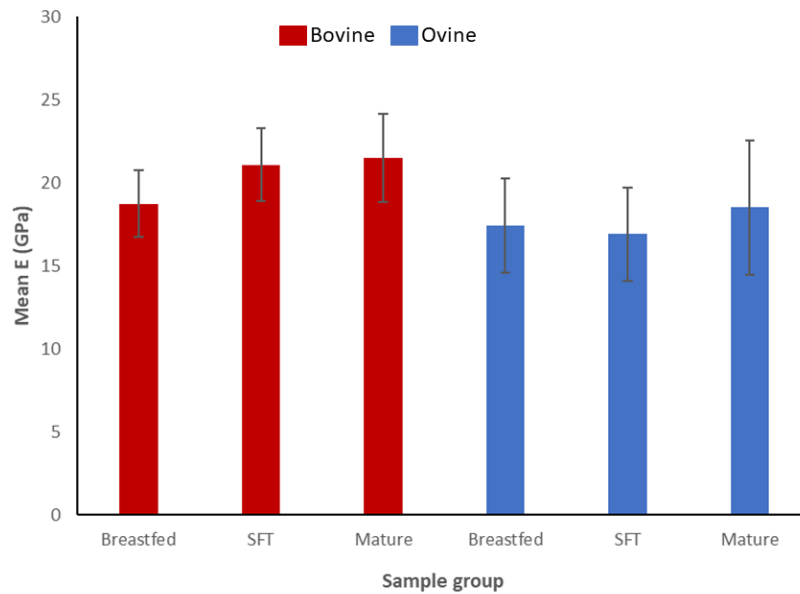


Figure 19. Bar chart representing the mean value of Young's modulus (E) with the respective standard deviations for the analyzed samples. Bovine specimens are displayed with red-coloured bars, while ovine specimens are represented in blue. SFT refers to solid-food-transitioning specimens.

By analyzing the data plotted above, it is possible to discern that there is a clear trend of increasing elastic modulus with age for juvenile specimens, which is the scope of this research project. It is common knowledge that, as it happens for human beings, the younger the subject, the lower the elastic modulus of the bone is and, consequently, the more elastic these tissues will be. Moreover, these results are consistent with publications in the literature, as reported by *Subit et al.* in their study on pediatric, adult, and elderly bone material properties [7], among others. The Young's modulus increase with age is applicable for both bovine and ovine specimens, so it can be stated that there is a common trend across species when evaluating this mechanical property.

5.4 Compositional Analysis

In order to perform this study, an energy dispersive X-ray (EDX) detector attached to the SEM was used. This method involves the analysis of X-rays with characteristic energies of the atoms present in the specimen, emitted when an incident electron hits the sample surface [6]. EDX allows to obtain both qualitative and quantitative information on the sample's composition since each detected X-ray's energy is characteristic of the element that emitted it. The result is a composition spectrum, as the one displayed in Figure 20.

As introduced in the first section, bone is a composite material consisting of both inorganic and organic components. The inorganic component is primarily crystalline hydroxyapatite, $[\text{Ca}_3(\text{PO}_4)_2]3\text{Ca}(\text{OH})_2$, whereas the organic components of bone include more than 30 proteins, being type I collagen the most abundant. This inorganic part also contains impurities and the most common one is carbonate in place of the phosphate groups. Other known substitutions may include potassium, magnesium, strontium, and sodium in place of the calcium ions, and chloride and fluoride in place of the hydroxyl groups [16].

EDX microanalysis of bone should include calcium, phosphorous, sulfur, magnesium, sodium, and carbonate salts [17], which is consistent with the elements displayed in the chart below and Table 4. These chemical elements were incorporated during animal bone development although the Ca/P ratio may vary according to nutritional conditions.

Eighteen samples were analyzed in this testing stage to address juvenile bone composition and how it varied within the different evaluated age ranges.

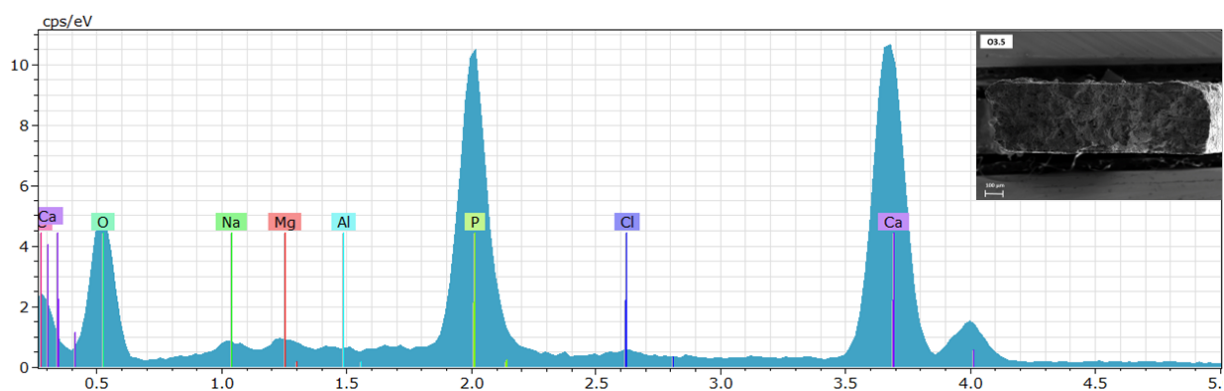


Figure 20. Compositional spectrum of O3.5 sample surface fracture obtained using EDX technique.

Sulfur is mainly found in tissues that contain high amounts of protein. It is a constituent of collagen, a protein that can be found in connective tissue, bones, and teeth. Even though it is a constituent element of the aforementioned protein, only small proportions of sulfur were reported on the as-studied bone specimens. In fact, it was not detected in all the analyzed samples.

Nechlich and Richards [18] performed sulfur isotope measurements of bone collagen from archaeological sites in their study, stating that the mean amount of sulfur in mammals was $0.28 \pm 0.08 \%$, which is consistent with the detected quantities provided by the EDX analysis.

Regarding the results, it can be observed that small percentages of aluminium were also detected in many of the samples. The presence of this element may be due to a couple of different reasons. On the one hand, aluminium is naturally present in large quantities in soils, but as insoluble complexes, which are not available for plants and therefore do not represent a problem for animals. The *American Association of Pediatrics (AAP)* considers that aluminium will only represent an important risk for health when aluminium's sulfate is used as a flocculant in public waters [19]. Even almost all the consumed aluminium passes through the gastrointestinal tract unabsorbed, and dietary intake quantities are really low, around 4 % of the aluminium content of the diet is retained and might partially be accumulated in bones. But, on the other hand, the presence of this element could be also attributed to a secondary signal coming from the stub used for sample insertion during the compositional analysis.

Additionally, it is worth mentioning that small strontium contributions were detected by the EDX, but since the intensity was that low, they have not been considered in the overall analysis. However, Sr can get into mammals' bodies through diet, since it is present in water and consequently in vegetables. Strontium can be considered a trace metal in mammals; it displays a chemical behaviour similar to that of calcium and it can have different protein linking grades. Cations Sr^{+2} can equimolarly be exchanged with calcium and therefore embodied into hydroxyapatite crystals [20].

Sodium and chlorine contributions were detected as well. As previously mentioned, these are expected findings, but most of the percentages reported in this study may probably come from the saline solution in which the samples were preserved in the fridge.

On the contrary, carbon content did not seem to follow a clear trend path. If samples of elderly animals were analyzed, C percentages would probably increase with age, since the atoms of this element will compensate for the missing Ca and P ones. However, it is important to note that carbon content values are probably higher than what they should be because a layer of this element was deposited on the samples' surfaces before their observation on the SEM. Moreover, carbon tape was used to attach the coupons to the microscope stubs, so contributions of the aforementioned may be expected as well.

Magnesium mass percentages did not follow a common trend and the variation was not relevant compared to that of calcium or phosphorous.

Table 4. Compositional analysis results obtained for eighteen samples using EDX. Results are displayed with its respective standard deviations.

Sample ID	C	O	Na	Mg	Al	P	Cl	S	Ca
V1.2	18.36±0.62	38.52±0.36	0.81±0.03	0.62±0.01	0.05±0.01	12.81±0.19	0.10±0.007	-	28.72±0.46
V1.3	15.12±1.08	28.36±2.13	0.57±0.08	0.35±0.04	-	14.50±0.5	0.27±0.02	-	40.40±2.96
V1.4	18.94±1.87	29.55±2.12	0.839±0.23	0.41±0.05	0.38±0	13.39±0.81	0.253±0.08	-	36.08±3.10
V2.2	16.13±1.19	30.52±2.38	0.64±0.08	0.44±0.05	0.10±0.005	14±0.76	0.17±0.04	-	38.11±3.05
V2.4	15.45±1.38	30.08±2.26	0.76±0.10	0.42±0.04	0.179±0	13.93±0.89	0.256±0.02	-	39.12±3.55
V2.5	16.59±1.23	33.37±1.88	0.67±0.07	0.37±0.04	0.03±0.01	14.050±0.58	0.21±0.03	-	34.70±2.34
V3.2	15.23±2.17	27.56±2.97	0.79±0.23	0.35±0.05	0.49±0.26	12.78±1.28	0.186±0.04	-	42.61±4.28
V3.3	14.95±1.93	24.33±1.57	0.43±0.08	0.24±0.04	0.07±0.01	16.67±0.65	0.22±0.07	0.16±0	42.93±2.08
V3.5	18.91±2.34	29.20±1.38	0.433±0.06	0.26±0.04	0.20±0.08	13.99±0.98	0.21±0.02	-	36.80±2.35
O1.2	13.75±0.69	31.92±1.09	0.57±0.05	0.40±0.02	0.04±0.01	16.01±0.43	0.34±0.02	-	36.96±1.16
O1.3	38.53±2.75	25.67±2.01	0.42±0.07	0.19±0.02	-	13.22±0.89	1.20±0.15	0.77±0.18	31.50±2.05
O1.5	20.94±2.31	32.13±1.40	0.73±0.07	0.36±0.036	0.14±0.06	13.54±0.05	0.45±0.05	-	31.70±2.31
O2.2	16.24±1.6	36.06±0.69	0.64±0.05	0.56±0.03	0.34±0.3	13.92±0.61	0.28±0.02	-	31.95±1.43
O2.3	12.55±0.86	31.56±1.43	0.70±0.11	0.48±0.04	1.12±0	15.91±0.56	0.49±0.06	-	38.61±1.8
O2.5	17.38±1.94	29.64±1.65	0.67±0.07	0.48±0.04	0.04±0.01	14.78±0.54	0.43±0.13	0.33±0	36.26±1.87
O3.2	16.84±1.25	31.51±1.37	0.49±0.045	0.36±0.04	0.08±0.01	14.67±0.41	0.13±0.02	-	35.93±1.28
O3.4	21.45±0.91	42.33±1.76	1.45±0.08	0.84±0.02	0.43±0.03	11.81±0.83	0.25±0.05	0.20±0	21.25±1.66
O3.5	13.96±2.63	33.71±3.64	0.62±0.13	0.33±0.08	0.02±0.01	10.54±1.26	0.22±0.05	-	40.61±5.8

Elastic modulus and bone strength positively correlate with age in juvenile bone tissue. A study by *Akkus et al.*, in which female rat femurs of 3 months old, middle-aged 8 months old, and 24 months old were analyzed using Raman spectroscopy, demonstrated that increased mineralization and increased crystallinity significantly correlated with decreased elastic deformation with age [21]. Also, *Yerramshetty et al.* studied the association between mineral crystallinity and the mechanical properties of human cortical bone. Their results revealed that increased tissue-level strength and stiffness positively correlated with increased crystallinity, while ductility was reduced. Moreover, the authors concluded that crystallinity could be used as a complementary diagnostic marker for the prediction of bone strength [22]. Additionally, *Currey et al.* studied the effect of variations in mineral content and Young's modulus of some mammalian mineralized tissues to discuss the implications for the variation of mineralization in nature. From their results, they concluded that, generally, in mineralized tissues, mineral content is associated with a higher elastic modulus but a lower toughness [23].

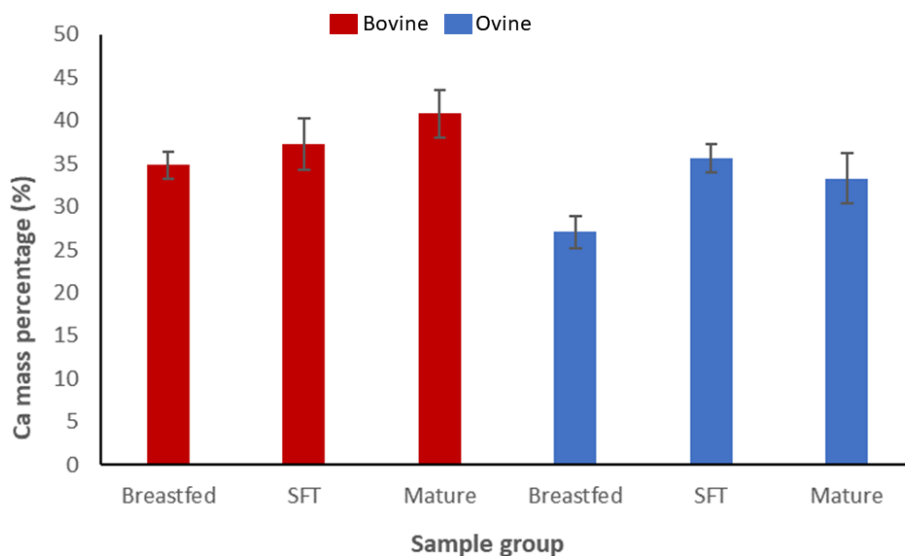


Figure 21. Calcium mass percentages reported with EDX analysis with their respective standard deviations. Bovine specimens are displayed with red-coloured bars, while ovine specimens are represented in blue. SFT refers to solid-food-transitioning specimens.

By observing the data displayed in Table 4 and that plotted in the previous figure, it has been found that the content of this element increases with age for juvenile bovine and ovine bone tissue. It can be noted that for the mature ovine group, the percentage of Ca obtained was slightly lower compared to the solid-food-transitioning specimens. However, its high standard deviation (± 2.91) could explain this anomaly, which was as well observed in the nanoindentation test results. Values for bovine samples ranged between 34 % and 41 % of Ca content, whereas for ovine specimens' results were between 33 % and 36 % (for breastfed to mature samples, respectively). The latter showed lower values which could be related to higher porosity contents.

When performing the fractographic analysis, it was possible to observe that ovine bone samples exhibited higher porosity than those coming from bovine specimens, therefore contributing to a lower mineral bone density.

Variations in calcification and, consequently, crystallinity, appear to be small for our samples, but large enough to contribute to mechanical properties variation. From previous results of this research project, it was verified that both elastic modulus and bone strength increased with age in juvenile tissue, being these numbers consistent with the compositional analysis results and with values reported in the literature. Moreover, it is possible to discern that it seems to be a fashion across species since the trend is common for both bovine and ovine bone specimens.

6. Conclusions

Throughout this document, coupons made out of cortical bone tissue from two different species (bovine and ovine) were evaluated in order to address how mechanical and chemical properties varied within three different juvenile age groups. A wide range of tests was performed to quantify whether the change in mechanical properties at different developmental stages is related to the change in bone tissue composition in a similar fashion across species.

Bone coupons were cut out and fabricated from juvenile bovine and ovine long bone specimens. Once the samples were prepared, they were subjected to tensile tests which allowed to mechanically characterize them, obtaining values of maximum strength, maximum stress, and maximum strain. A completely new experimental set-up was designed so that misalignment between the top and the bottom ends of the coupons was avoided. Not all the tested samples broke in the cane, so the aforementioned mechanical properties were only provided for those which experienced fracture in the gage area. Results from tensile tests revealed that both strength and stress increased with age in juvenile bone tissue, reaching values in the range of 25-29 MPa for bovine breastfed samples, and 35 MPa for solid food transitioning, and 42 MPa for the mature bovine sample. On the other hand, these properties were not able to be quantified for ovine bone specimens, since only one of these samples broke in the cane area, reaching an unusually high maximum stress value of 90 MPa and experiencing signs of plastic deformation, as it can be determined from its stress-strain curve. Stress curves of bovine samples revealed that their global fracture behaviour was linear elastic.

Moreover, it was possible to corroborate the previous results by performing a fractographic analysis of the five samples that broke in the cane area. By observing the surface fracture of the aforementioned, it was concluded that bovine bone coupons experienced signs of brittle fracture, with very clean surfaces and is possible to address in most cases the crack growth direction. On the other hand, the mature ovine specimen showed micro deformation features, which are typical of fractures that experienced plastic deformation.

In addition, a set of nanoindentation tests were conducted so as to determine bone coupons' elastic modulus and understand how this mechanical property varied within the analyzed age groups. Results showed that Young's modulus increased with age for both species, with values ranging between 18 and 20 GPa, which are consistent with literature numbers for cortical bone specimens.

Lastly, a compositional analysis was performed on a large group of samples to identify bone tissue's elemental composition and to check if changes in chemical composition were related to the mechanical properties' variation. Energy Dispersive X-ray analysis detected expected compositional findings.

By analyzing the results, it was possible to confirm that calcium mass percentage, and therefore the mineralization and crystallization of the bones, increased with age for juvenile tissue in both animal species. The latter confirms previous literature findings, which stated that increases in the degree of calcification and crystallinity were positively correlated with bone strength and elastic modulus. Juvenile bone tissue becomes stiffer and more resistant to fracture with increasing age. Moreover, it can be confirmed that there is a trend across species since bovine and ovine bone coupons behaved in a very similar way.

It has been established that juvenile bone shows different mechanical behavior from that of adult bone, in which in general, the older the subject, the lower the mechanical properties. Despite some recent studies on the matter, the characterization of juvenile bone tissue remains poorly documented. The aim of the present work is to gain insight into the mechanical and compositional properties of growing cortical bone tissue to improve the knowledge of juvenile bone to cope with the existing practical difficulties of testing human pediatric tissue. Additionally, these results provide the foundation for exploring alternative methods to scale material properties for different age ranges based on more extensive animal tissue.

6.1 Future work

In order to obtain more consistent results, it will be necessary to fabricate and test more specimens using the in-home developed tensile testing set-up. A possible improvement that could be introduced to avoid coupon breakage on the heads, will be to reduce the width of the gauge area so that stresses are mainly concentrated in that area.

Moreover, the resolution of the as-recorded tensile testing videos needs to be improved so that the point cloud tracks can be correctly performed by the digital imaging correlation software. Bringing the camera closer to the tested specimen and increasing image resolution will help to get better results.

Regarding the compositional analysis with SEM, it will be interesting to coat the samples with a gold layer instead of a carbon one. SEM working principle uses electrons to create images, so as previously explained, a layer of a conductive material needs to be deposited on biological tissues for it to be inspected. The fact of using Au instead of C will lead to more accurate compositional results since the C content in the bone tissue is masked by the carbon conductive layer.

7. References

- [1] H. Leng, M. J. Reyes, X. N. Dong, and X. Wang, "Effect of age on mechanical properties of the collagen phase in different orientations of human cortical bone," *Bone*, vol. 55, no. 2, pp. 288–291, 2013, doi: 10.1016/j.bone.2013.04.006.
- [2] X. Wang, X. Shen, X. Li, and C. Mauli Agrawal, "Age-related changes in the collagen network and toughness of bone," *Bone*, vol. 31, no. 1, pp. 1–7, 2002, doi: 10.1016/S8756-3282(01)00697-4.
- [3] E. A. Zimmermann, B. Busse, and R. O. Ritchie, "The fracture mechanics of human bone: influence of disease and treatment," *BoneKEy Reports*, vol. 4, no. June, pp. 1–13, 2015, doi: 10.1038/bonekey.2015.112.
- [4] M. J. Mirzaali *et al.*, "Mechanical properties of cortical bone and their relationships with age , gender , composition and microindentation properties in the elderly," *Bone*, vol. 93, pp. 196–211, 2016, doi: 10.1016/j.bone.2015.11.018.
- [5] E. Lefèvre *et al.*, "Compositional and mechanical properties of growing cortical bone tissue : a study of the human fibula," pp. 1–16, 2019, doi: 10.1038/s41598-019-54016-1.
- [6] E. Donnelly, "Methods for assessing bone quality: A review," *Clinical Orthopaedics and Related Research*, vol. 469, no. 8, pp. 2128–2138, 2011, doi: 10.1007/s11999-010-1702-0.
- [7] D. Subit, C. Arregui, R. Salzar, and J. Crandall, "Pediatric, adult and elderly bone material properties," *2013 IRCOBI Conference Proceedings - International Research Council on the Biomechanics of Injury*, pp. 760–769, 2013.
- [8] A. Standards, "Standard Practice for Verification of Specimen Alignment Under Tensile Loading," *ASTM Book of Standards*, pp. 1–8, 1999.
- [9] U. de Málaga, "Microscopía Electrónica de Barrido," 2016. <http://www.scai.uma.es/areas/micr/sem/sem.html>
- [10] C. E. Hoffler, X. E. Guo, P. K. Zysset, and S. A. Goldstein, "An Application of Nanoindentation Technique to Measure Bone Tissue Lamellae Properties," vol. 127, no. December 2005, 2016, doi: 10.1115/1.2073671.
- [11] I. N. Sneddon, "The relation between load and penetration in the axisymmetric boussinesq problem for a punch of arbitrary profile," *International Journal of Engineering Science*, vol. 3, no. 1, pp. 47–57, 1965, doi: 10.1016/0020-7225(65)90019-4.
- [12] W. Oliver and G. Pharr, "An improved technique for determining hardness," *Journal of Materials Research*, vol. 7, no. 6. pp. 1564–1583, 1992.
- [13] R. M. Pidaparti and A. Vogt, "Experimental investigation of Poisson ' s ratio as a damage parameter for bone fatigue," 2001.
- [14] M. L. Oyen, "Nanoindentation hardness of mineralized tissues," *Journal of Biomechanics*, vol. 39, no. 14, pp. 2699–2702, 2006, doi: 10.1016/j.jbiomech.2005.09.011.

- [15] M. Casanova, A. Balmelli, D. Carnelli, D. Courty, P. Schneider, and R. Müller, "Nanoindentation analysis of the micromechanical anisotropy in mouse cortical bone," 2017.
- [16] X. Feng, "Chemical and Biochemical Basis of Cell-Bone Matrix Interaction in Health and Disease," vol. 3, no. 2, pp. 975–990, 2010, doi: 10.2174/187231309788166398.Chemical.
- [17] G. A. da Cruz, T. de Sérgio, E. A. Sallum, and A. F. M. de Lima, "Morphological and chemical analysis of bone substitutes by scanning electron microscopy and microanalysis by spectroscopy of dispersion energy," *Brazilian Dental Journal*, vol. 18, no. 2, pp. 129–133, 2007, doi: 10.1590/s0103-64402007000200008.
- [18] O. Nehlich and M. P. Richards, "Establishing collagen quality criteria for sulphur isotope analysis of archaeological bone collagen," pp. 59–75, 2009, doi: 10.1007/s12520-009-0003-6.
- [19] J. Méndez, "Metales pesados en alimentación animal," *XVII Curso de Especialización FEDNA*, pp. 1–5, 2002.
- [20] V. J. Picón- Borregales D, Carrero PE, Gutiérrez- Peña LV, "Relationship between strontium, bone mineral metabolism and osteoporosis. A literature review," *Avan Biomed*, vol. 6, no. 2, pp. 133–143, 2017.
- [21] O. Akkus, F. Adar, and M. B. Schaffler, "Age-related changes in physicochemical properties of mineral crystals are related to impaired mechanical function of cortical bone," vol. 34, pp. 443–453, 2004, doi: 10.1016/j.bone.2003.11.003.
- [22] J. S. Yerramshetty and O. Akkus, "The associations between mineral crystallinity and the mechanical properties of human cortical bone," *Bone*, vol. 42, no. 3, pp. 476–482, 2008, doi: 10.1016/j.bone.2007.12.001.
- [23] J. D. Currey, K. Brear, and P. Zioupos, "Notch sensitivity of mammalian mineralized tissues in impact," *Proceedings of the Royal Society B: Biological Sciences*, vol. 271, no. 1538, pp. 517–522, 2004, doi: 10.1098/rspb.2003.2634.